Elucidation Of Properties In Langmuir Monolayers And Langmuir - Blodgett (LB) Films Formed By Calix[6]arene

Darvina Lim C.K.[1] and Faridah L. Supian[2,*]

[1,2] *Department of Physics, Faculty of Science and Mathematics, Sultan Idris Education University (UPSI), 35900 Tanjong Malim, Perak, Malaysia.*

**Email: faridah.lisa@fsmt.upsi.edu.my*

(Received: 09 01 2017; published 08 09 2017)

Abstract. One-molecule-thick monolayer that assembled by insoluble organic material spread on an aqueous subphase, normally water subphase is known as Langmuir monolayer. Meanwhile, Langmuir-Blodgett (LB) film is a single or multiple layers of Langmuir monolayer being deposited onto a solid substrate. In this work, the characterization of calix[6]arene (*C6*) was studied using LB technique, surface potential meter, and UV-Visible (UV-Vis) spectrometer. From surface pressure-area isotherms, the limiting area per molecule and radius of the molecule were decreased with the increment of spreading volume. Effective dipole moments were determined from surface potential values using Helmholtz equation. Later, the maximum surface potential was obtained. In addition, UV-Vis spectroscopy demonstrated that peak absorbance of *C6* occurred at 282nm with one "shoulder" peak exist at 275nm. Surface topography studied by Field Emission Scanning Electron Microscope also demonstrates nearly uniform *C6* layers. Hence, some characteristic of *C6* was elucidated in this study and this material shall be further studied for practical applications such as ion sensing.

Keywords: Calix[6]arenes, Langmuir-Blodgett, surface pressure-area, surface potential, effective dipole moment

I. INTRODUCTION

Calixarenes are known as the third generation of supramolecules after cyclodextrins and crown ethers [1]. They generally formed by the phenol units that bridged by alkylidene group to form a cyclic oligomer. Calixarenes can interact or form the complex with the other ions or molecules in their host-guest interaction, give rise to the molecule and ion-sensing application [2].

In general, calixarenes are the amphiphilic molecule that insoluble in water but soluble in organic solvents, hence they can form a monolayer in the air/water interface and being studied through the Langmuir-Blodgett (LB) technique. Recent studies about calixarenes being deposited into Langmuir-Blodgett film for application included the calix[4]arene derivatives for the chloroform gas sensing application and the calix[6]arene derivatives on organic vapor sensing done by Ozmen's group [3,4]. Besides that, there is another study about calix[6]arene derivative

in Langmuir films at the water/air interface [5] using Brewster Angle Microscopy and Molecular Dynamic simulations.

In this work, the basic calix[6]arene is being studied through the LB technique, surface potential probe, UV-Visible (UV-Vis) spectrometer and Field Emission Scanning Electron Microscope (FESEM) to identify some of its monolayer and thin film properties. This work is conducted to get some insight into the behavior and formation of the *C6* monolayer, plus the formation of the thin film when being compressed in water/air interface and transfer to a solid substrate through LB method.

II. MATERIALS AND METHOD

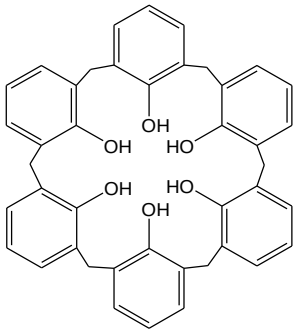

FIGURE 1. Chemical structure of *C6* ($C_{42}H_{36}O_6$)

Basic material in this study is calix[6]arene-37, 38, 39, 40, 41, 42-hexol (*C6*) (Figure 1) that purchased from Sigma-Aldrich. 2 mg of *C6* was dissolved in 10 ml of chloroform ($CHCl_3$) (Sigma-Alrich) that acted as the organic solvent to produce 0.2 mg/ml of solution. No further purification process needed for *C6* and chloroform.

Quartz (2.5 cm × 2.5 cm) was selected as the substrate for thin film deposition. Firstly, Decon 90 was utilized to gently clean the substrates and later rinsed with deionized (DI) water. Then, the substrates were ultrasonicated with acetone (10 minutes), propanol (10 minutes) and DI water (2 minutes) before dried with a nitrogen gun. Lastly, substrates were arranged in tilted vertical position in a beaker and sealed with 1,1,1,3,3,3-Hexamethyldisilazane ($C_2H_{19}NSi_2$) for overnight to develop hydrophobic property on the substrate's surface as to enhance the attachment of *C6* monolayer on it.

III. CHARACTERIZATION

LB technique was practiced in this work to study the properties of the *C6* monolayer on air/water interface. A commercially obtainable medium-sized KSV NIMA 2002 System 2 LB deposition trough with a sensitivity of ±0.001 mN/m was employed. This instrument has a hydrophobic Teflon trough with 570 × 150 mm^2 effective film area and two hydrophilic Delrin barriers. Deionized water (Sartorius Stedim Biotech) with an 18.2 MΩ resistivity was filled into the trough as the subphase. Micro-aspiration was performed to ensure the water surface free from any dust or particles that would alter the result. Filter paper acted as the pressure sensor to detect surface pressure. For surface pressure-area (*Π-A*) isotherm measurement, 100 µl of the solution was evenly spread in small droplets on the subphase using SGE Analytical Science Microlitre

Syringe. 15 minutes were allocated for the solvent evaporation and *C6* molecules' equilibration arrangement process, thus allowed only the *C6* molecules uniformly float on the subphase's surface. Afterward, the *C6* monolayer was symmetrically compressed by barriers from both sides at 12 mm/min.

In addition, a KSV SPOT1 probe with a sensitivity of 1 mV was employed to determine the surface potential (ΔV) of the *C6* monolayer with different spreading volume using vibrating plate capacitor method. A stainless steel plate acts as the counter electrode was placed under the sub phase and attached to the probe. A small uniform distance of about 1 mm was ensured between the monolayer and the vibrating plate. All the data simultaneously feedback to the KSV software in a computer as the compression process was performed. *Π-A* isotherm and surface potential-area (ΔV-*A*) isotherm graphs were plotted from the data. Standard trough cleaning practice was applied between different spreading volume measurements (125 µl – 175 µl) of *C6* later.

20 layers of *C6* monolayer were developed on the substrate through vertical dipping method in Y-type LB deposition [6]. From the *Π-A* isotherm graph, 20 mN/m was chosen as the deposition pressure since the monolayer existed in "solid" state at this surface pressure. 5 mm/min was applied for the upward and downward dipping stroke speed. 10 minutes was allowed for each upward stroke in the air to ensure the drying process of the thin film took place.

Several optical absorption properties of *C6* either in solution or thin film form were determined with Agilent 8453 UV-Visible (UV-Vis) Spectroscopy. The calixarene solutions have a serial dilution from 0.10 mg/ml to 0.02 mg/ml with a decrement of 0.02 mg/ml. The diluted *C6* solution has less noise on the absorbance spectra. This dilution has been carried out to study the molar absorptivity of the *C6* solution.

Besides that, the *C6* thin film is being observed using Field Emission Scanning Electron Microscope (FESEM) to study the surface morphology and structure of *C6* at the 5K magnitude. This work is conducted at room temperature.

IV. RESULTS AND DISCUSSION

A. Surface Pressure- Area (*Π-A*), Surface Potential- Area (ΔV-*A*) and Effective Dipole Moment- Area ($\mu_{\perp}$-*A*) Isotherm.

C6 monolayers were studied through *Π-A* isotherm graph (Figure 2) that illustrated the surface pressure as a function of the molecular area at the air/water interface. For *C6* monolayer, the hydrophilic hydroxyl group (-*OH*) bonded at phenol units are expected to be in contact with the aqueous subphase, whilst the hydrophobic aromatic hydrocarbon groups are pointing to the air [7].

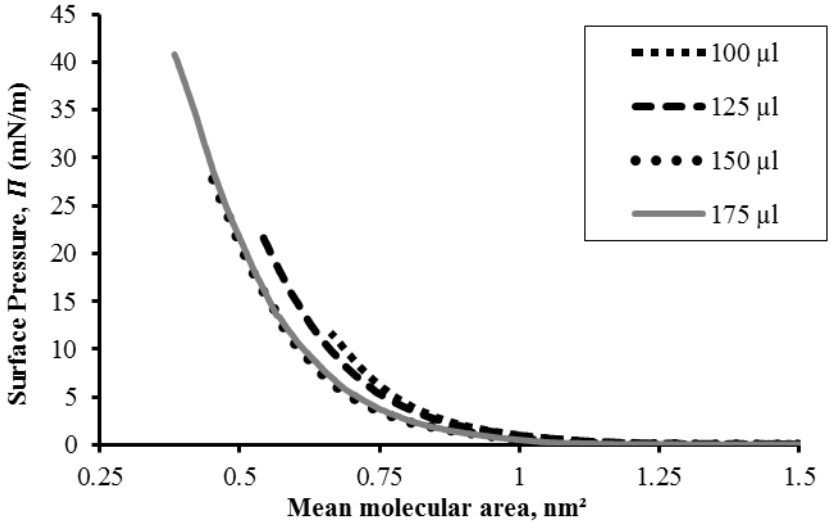

FIGURE 2. *Π-A* isotherm graph for *C6*

In this work, *Π* is defined as the surface tension difference between the surface of clean subphase and *C6* monolayer-subphase surface. As the spreading volume increased, the *Π-A* isotherm curve being shifted to the left due to intermolecular packing. The small spreading volume of *C6* (100µl) formed incomplete monolayer formation. With the increment of spreading volume, the *Π-A* isotherm curves achieved a complete monolayer formation, thus the estimated optimal mean molecular area can be deduced by extrapolating the steepest linear region of the curves to the zero surface pressure. Estimated radius of the *C6* molecule was determined by assuming the cross-sectional area of the molecule is a circle. From *Π-A* isotherm graphs, the limiting area per molecule and radius of the molecule were observed decreases with the increment of spreading volume. According to Table 1, the most optimal mean molecular area and radius per *C6* molecule are about 0.615 nm^2 and 0.422 nm. The mean molecular area also considered as the "maximal possible area of cross-section" for the *C6* molecule sphere at the air/water interface [7].

One of the significant methods to analyze the electrical structure of the material surface is ΔV method [8]. For this work, the ΔV is defined as the potential difference between the surface of clean subphase and *C6* monolayer-subphase surface [8]. ΔV can be correlated to the average effective dipole moment ($\mu_{\perp}$) of *C6* monolayer molecules through Helmholtz equation (1) as shown below:

$$\mu_{\perp} = \varepsilon_0 \varepsilon_r A \Delta V \quad (1)$$

where $\mu_{\perp}$ is the effective dipole moment, ε_0 and ε_r are the vacuum permittivity (8.854×10^{-12} $C^2N^{-1}m^{-2}$) and relative permittivity for the monolayer between the electrodes and lastly A is the area per molecule in m^2.

Since the relative permittivity of the monolayer is unknown, ε_r is assumed to be 1 in this study due to the large difference between the thickness of the *C6* monolayer and the thickness of air gap between the monolayer and vibrating plate [9]. The calculated $\mu_{\perp}$ values were expressed in Debye unit (D). The calculated $\mu_{\perp}$ values were used to plot the $\mu_{\perp}$ curves in each of their respective ΔV-*A* isotherm graphs as visualized in Figure 3 except for 100 µl spreading volume of

C6 due to insufficient monolayer formation. The maximum ΔV (ΔV_{max}) values were obtained by identified the maximum $\mu_{\perp}$ ($\mu_{\perp max}$) values in Figure 3.

As visualized in Figure 3(c), the ΔV increased long before the Π increased since compression process started. At zero Π, the monolayer in a gaseous state before transited into a liquid-expanded and liquid-condensed state (~ 1-19 mN/m), lastly the solid state (~ 19 mN/m). Flexures occurred in ΔV and $\mu_{\perp}$ when monolayer transited from a gaseous state to liquid state. Changes in orientation being observed as the ΔV and $\mu_{\perp}$ increased. The runs of $\mu_{\perp}$-*A* isotherm suggested that *C6* molecules lied almost horizontally on the interface when a large mean molecular area is available. However, as the compression process initiated, the interaction between molecules happened caused the lifting of the hydrophobic part of molecules took place. This gave rise to the molecule's tilted alignment with respect to the horizontal direction. A similar result also reported in [10] for azo dye/liquid crystal mixtures monolayer.

(a) 125 µl of *C6*

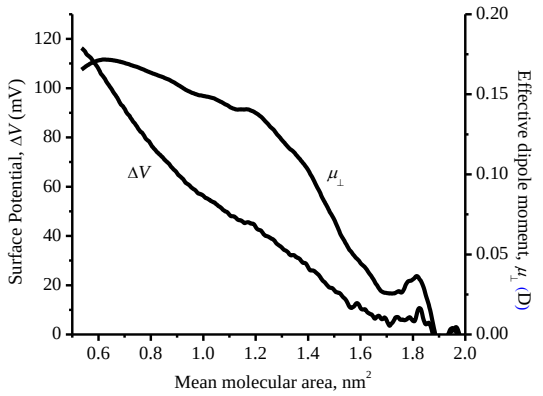

(b) 150 µl of *C6*

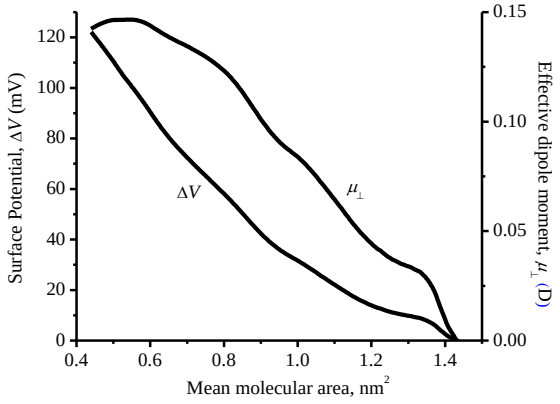

(c) 175 µl of *C6*

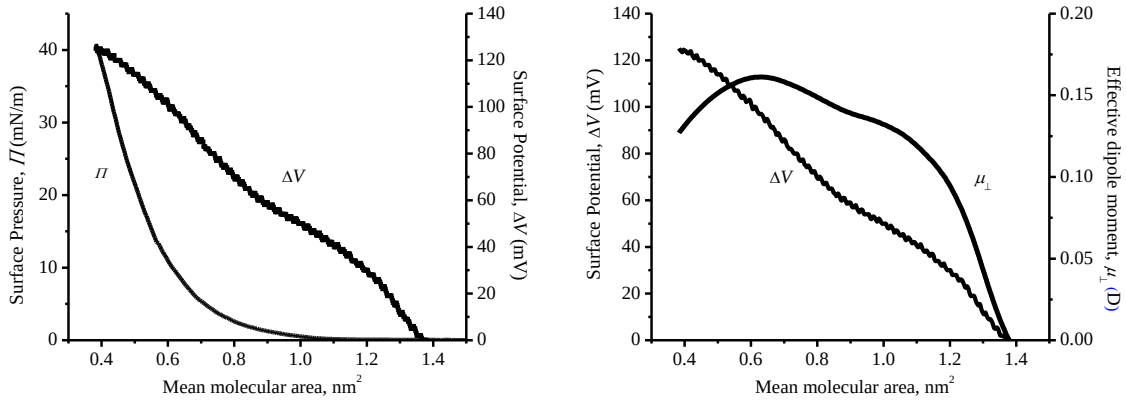

FIGURE 3. (a) – (b) ΔV-*A* and $\mu_{\perp}$-*A* isotherm graphs for *C6* and **(c)** Π-*A*, ΔV-*A* and $\mu_{\perp}$-*A* isotherm graphs for 175 µl of *C6*

TABLE 1. Data from *Π-A*, ΔV*-A* and $\mu_{\perp}$*-A* isotherm graphs for *C6* Langmuir monolayer

Volume (µl)	Mean molecular area (nm^2)	Radius (nm)	ΔV_{max} (mV)	$\mu_{\perp max}$ (D)
100	0.827	0.513	-	-
125	0.719	0.478	104	0.172
150	0.635	0.450	102	0.147
175	0.615	0.442	97	0.161

B. UV- Visible (UV-VIS) Absorbance Results

The UV absorption of the *C6* solutions with different dilution was illustrated in Figure 4. From the figure, *C6* has a peak absorbance at 282 nm and a "shoulder" peak at 275 nm. The peaks are attributed to π-π* and n-π* transition [11,12]. Although the *C6* solution has another "shoulder" peak at 240 nm, this peak should not be considered as the "cut-off" wavelength for $CHCl_3$ is below 245 nm for 1cm path length [13].

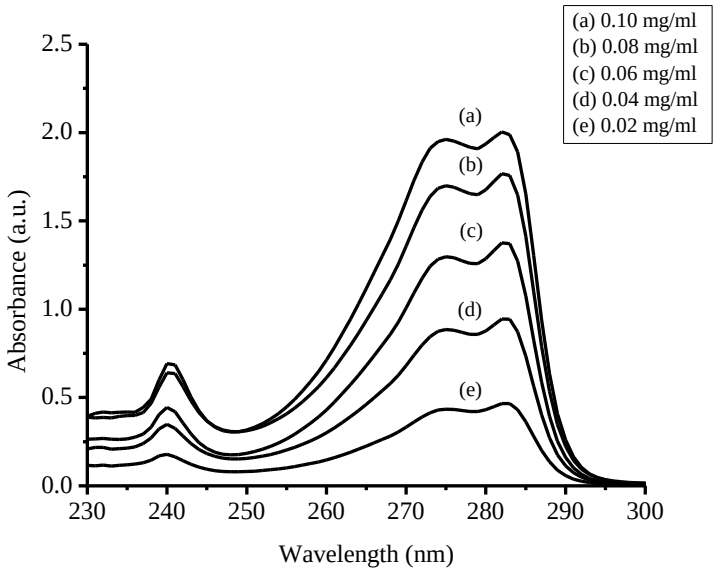

FIGURE 4. UV-Vis absorbance spectra of *C6* solution with different concentration

The molar absorptivity of *C6* was calculated for the absorbance peaks and "shoulder" peak as demonstrated in Figure 5 and Table 2 through Beer-Lambert Law (2),

$$\varepsilon = \frac{A}{bc} \tag{2}$$

where ε is the molar absorptivity (Lmol-1cm-1), A is the absorbance, b is the solution path length (1 cm in this study) for the light to travel and c is the concentration of the solution (molL-1). The absorbance data plotted in Figure 5 has error bars indicating standard deviation around the mean.

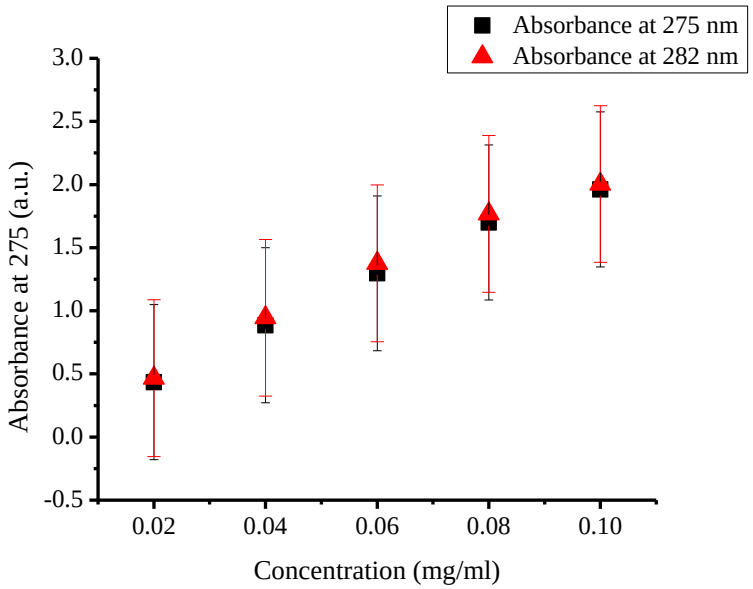

FIGURE 5. UV-Vis absorbance versus concentration of *C6* solution

TABLE 2. Molar Absorptivity of *C6* solution

Absorbance Peak (nm)	Molar Absorptivity ($Lmol^{-1}cm^{-1}$)
275	12314
282	12415

Deposition of the thin film onto the quartz from *C6* monolayer was studied through the UV-Vis absorbance spectra in Figure 6. This film was compared with 0.1 mg/ml of *C6* solution. The peak absorbance of the *C6* solution and *C6* thin film occurred at 282 nm and 283 nm respectively. The "shoulder" peak of both, *C6* solution and the thin film exist at 275 nm and 276 nm respectively. There is only slightly red shift in peak absorbance for *C6* thin film indicated that *C6* is stable although being deposited as a thin film since the fingerprint of *C6* still retained.

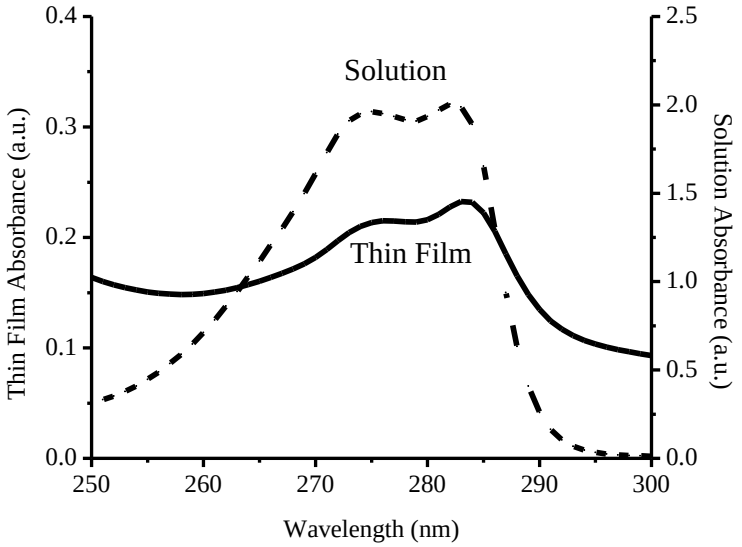

FIGURE 6. UV-Vis absorbance spectra of *C6* solution and thin film

C. SURFACE TOPOGRAPHY ANALYSIS

The topography of the *C6* thin film studied by FESEM is illustrated in Figure 7 below. Overall, the *C6* thin film showed a surface morphology with some parts of mountain-like structure. This mountain-like feature actually contributed by the insufficient space formed during the drying process [14].

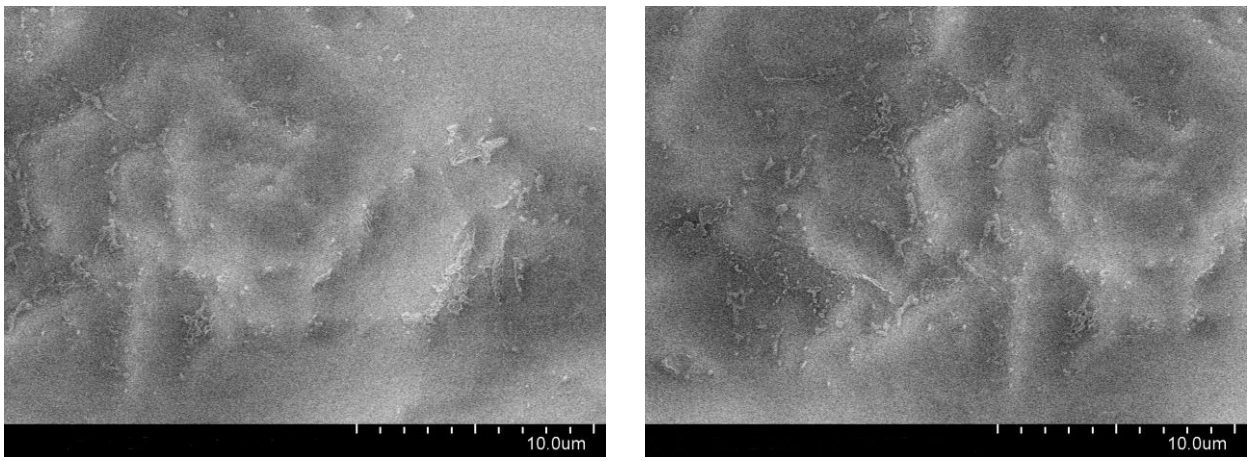

FIGURE 7. Surface morphology of *C6* thin film deposited on quartz

When the *C6* molecules being transferred onto quartz substrate, water molecules also adhere to the substrate and form a floating mechanism for the *C6* molecules. As the adhesion of water molecules formed a curve surface area as compared to the substrate, water provides a larger surface area for *C6* molecules to rearrange themselves more evenly. As the drying process take places, the surface area for *C6* molecules being reduced, thus causing the *C6* molecules to compresses with each other and start to slide at an angle toward the nearby calixarene molecules.

Hence, the compression due to insufficient space and molecule rearrangement result in the mountain-like feature morphology as seen in Figure 7.

Another reason is due to the HMDS layer that used to hydrophobic the quartz substrate. During the hydrophobic process, HMDS layer might attach to the quartz substrate in a less uniform pattern. This will caused the first layer of *C6* adhered to substrate start to develop wrinkle effect. By overlapping the *C6* layers, the wrinkle effect developed into larger scale mountain-like feature as displayed in Figure 7.

V. CONCLUSION

LB technique, ΔV probe, and UV-Vis spectroscopy were employed to study the characteristics of *C6*. From the *Π*-A isotherm, different phases of *C6* monolayer occurred and the solid phase of the monolayer was used to form the thin film. This thin film still retained the characteristic of *C6* after being studied by UV-Vis spectroscopy. The surface topography of *C6* thin film also showed a uniform surface. The *C6* thin film can be further explored into the potential application such as ion sensing.

Acknowledgements

The authors acknowledge RACE Research Grant (2014-0003-102-62), UPSI and MOHE for the financial support of this work. The authors are thankful for the instrumentation facilities provided by Physics Department and Chemistry Department, UPSI.

---

1. S. Shinkai, *Tetrahedron Report Number 340* **49**(40), 8933-8968 (1993).
2. H. J. Kim, M. H. Lee, L. Mutihac, J. Vicens and J.S. Kim, *Chem. Soc. Rev.* **41**(3), 1173-1190 (2012).
3. M. Ozmen et al., *Sens. Actuators, B Chemical* **190**, 502-511 (2014).
4. M. Ozmen, Z. Ozbek, M. Bayrakci, S. Ertul, M. Ersoz and R. Capan, *Appl. Surf. Sci*. **359**, 364-371 (2015).
5. L. S. de Lara, E. C. Wrobel, M. Lazzarotto, S. R. de Lázaro, A. Camilo Jr and K. Wohnrath, *Phys. Chem. Chem. Phys*. **18**, 22906-22913 (2016).
6. O. N. Oliveira Jr, *Braz. J. Phys.,* **22**(2), 60-69 (1992).
7. A. Turshatov, N. Melnikova, Y. Semchikov, I. Ryzhkina, T. Pashirova, D. Möbius and S. Y. Zaitsev, *Colloid Surface A* **240**(1-3), 101–106 (2004).
8. A. Ulman, *An introduction to ultrathin organic films from Langmuir-Blodgett to self-assembly*, San Diego: Academic Press, Inc, 1991, pp.21-22.
9. B. Korchowiec, A. B. Salem, Y. Corvis, J. B. Regnouf de Vains, J. Korchowiec and E. Rogalska, *J. Phys. Chem. B* **111**(46), 13231-13242 (2007).
10. D. Bauman, A. Plóciennik and K. Inglot, *Acta Phys. Pol. A* **116**(2), 203-210 (2009).
11. M. Ignat, A. Farcas, A. Vasile and E. Popovici, *Stud. Surf. Sci. Catal*. **174**A, 389-392 (2008).
12. M. Kobayashi et al., *Opt. Express*, **20**(22), 24856-24863 (2012).
13. J. W. Robinson, E. M. S. Frame and G. M. Frame, *Undergraduate Instrumental Analysis (7th Ed).* Boca Raton: CRC Press, 2014, pp. 370.

14. M. M. Jaafar, et al. *Langmuir,* **31**(38), 10426–10434 (2015).